(Fig. 3, A and B), show that in a narrow rf power window all the particles in the same picture have the same temporally chaotic motion and similar interparticle distances.

At higher rf powers, a more chaotic 3D collective excitation with typical frequencies from 10 to 20 Hz and a length scale of a few millimeters (Fig. 3, C and D) is observed. The fluctuations of particle velocity and density are associated with the fluctuations in the local plasma emission (the emission from the atoms excited by electron impact collisions), which is a function of electron density (*8*). Another typical state exhibits disordered motion (Fig. 3, E and F). In this state, the contribution from the long-wavelength coherent part is much weaker than those in Fig. 3, C and D. Note that in all the pictures of Fig. 3, the particle speeds (>2 cm/s) are much higher than those in the liquid state shown in Fig. 1B. The corresponding kinetic energies (for a particle with a 5-μm diameter, 1 cm/s corresponds to about 5 eV kinetic energy) are many orders of magnitude higher than that supplied by the background neutral gas, which is at room temperature.

The rf dusty plasma system is a typical stationary, nonequilibrium open system with finite boundaries. Nevertheless, the low energy states of our system exhibit hexatic phase and rotational cooperative motions with various scales similar to other 2D thermal systems (*12–14*). Our first observations of the coherent and chaotic couplings between dust particles and self-organized background plasma fluctuations are the interesting and unique features of this open system attributable to its high energy and less viscous low-pressure background. Note that although dust particles are unlikely to gain energy from electron collisions because of large differences in mass, they can coherently or stochastically gain large amounts of energy (>10 eV) from fluctuations of a few millivolts in the low-frequency electric field. This also shows that, in addition to the general interest in its crystal structure, phase transition, and dusty plasma waves, dusty plasma is a good system in which to study nonlinear wave-particle interactions and heavy-particle motion in a chaotic background (*15*).

REFERENCES AND NOTES

1. E. Wigner, *Trans. Faraday Soc.* **34**, 678 (1939).
2. S. Ichimaru, *Rev. Mod. Phys.* **54**, 1017 (1982).
3. H. Ikezi, *Phys. Fluids* **29**, 1764 (1986).
4. J. H. Chu and Lin I, *Physica A* **205**, 183 (1994).
5. ______, *Phys. Rev. Lett.* **72**, 4009 (1994).
6. Y. Hayshi and K. Tachibana, *Jpn. J. Appl. Phys.* **33**, 804 (1994).
7. H. Thomas *et al.*, *Phys. Rev. Lett.* **73**, 625 (1994).
8. J. H. Chu, J. B. Du, Lin I, *J. Phys. D* **27**, 296 (1994); Lin I, C. S. Chern, J. H. Chu, J. M. Liu, J. B. Du, *Physica A* **205**, 443 (1994).
9. C. K. Goertz, *Rev. Geophys.* **27**, 271 (1989).
10. J. H. Chu and Lin I, *Phys. Rev. A* **39**, 233 (1989); Lin I and J. M. Liu, *Phys. Rev. Lett.* **74**, 3161 (1995).
11. R. K. Varma, P. K. Shulka, V. Krishan, *Phys. Rev. E* **47**, 3612 (1993).
12. P. Choquard and J. Clerouin, *Phys. Rev. Lett.* **50**, 2086 (1983); M. M. Hurley and P. Harrowell, *Phys. Rev. E* **52**, 1694 (1995); V. A. Schweigert and F. M. Peeters, *Phys. Rev. B* **51**, 7700 (1995).
13. J. M. Kosterlitz and D. J. Thouless, *J. Phys. C* **6**, 1181 (1973); A. P. Young, *Phys. Rev. B* **19**, 1855 (1979); B. I. Halperin and D. R. Nelson, *Phys. Rev. Lett.* **41**, 121 (1978).
14. See, for example, K. J. Strandburg, Ed., *Bond-Orientational Order in Condensed Matter Systems* (Springer, New York, 1992).
15. C. Jarzynski, *Phys. Rev. Lett.* **74**, 2937 (1995).

16. This work was supported by the Department of Physics, National Central University, and the National Science Council under contract NSC-85-2112-M008-011.

24 January 1996; accepted 18 April 1996

Electrical Properties of the Venus Surface from Bistatic Radar Observations

Gordon H. Pettengill,* Peter G. Ford, Richard A. Simpson

A bistatic radar experiment in 1994, involving reception on Earth of a specularly reflected, linearly polarized 13-centimeter-wavelength signal transmitted from the Magellan spacecraft in orbit around Venus, has established that the surface materials viewed at low and intermediate altitudes on Venus have a relative dielectric permittivity of 4.0 ± 0.5. However, bistatic results for the Maxwell Montes highlands imply an electrically lossy surface with an imaginary dielectric permittivity of −*i* 100 ± 50, probably associated with a specific conductivity of about 13 mhos per meter. Candidates for highlands surface composition include ferroelectrics, a thin frost of elemental tellurium, or a plating of magnetite or pyrites.

Radio observations of the Venus highlands have revealed a surface material that exhibits radiothermal emissivity as low as 0.3 and normal-incidence radar reflectivity as high as 0.6 (*1*, *2*). These values are not characteristic of most of the Venus surface, for which the emissivity is about 0.85 and the reflectivity is about 0.15 (*2*). The abrupt change in emissivity and reflectivity in the highlands occurs above an altitude of about 6054 km near the equator, increasing to above 6055.5 km at high northern latitudes. Mechanisms proposed to explain this unexpected behavior include scattering and emission from a roughened high-dielectric interface (*2*) and low-loss volume scattering from within the surface (*3*). As more observations have accumulated, it has become difficult to find appropriate materials that can satisfy all the known constraints of the scattering models.

Bistatic radar observations, in which the transmitter and receiver are physically separated and thus view the surface from different directions, can yield more information on the scattering process than can the usual backscattering geometry, particularly if a full polarization description of the echo is available (*4*). Bistatic radar observation of Venus requires a spacecraft because the maximum angular separation of Earth-based transmitters and receivers as viewed from Venus is less than 1 minute of arc. We were fortunate that the Magellan spacecraft (*5*), in orbit around Venus since August 1990, became available for such observations in late 1993, as it concluded its primary mission objectives.

Constrained by the distance to Venus (1.3 astronomical units) and by the relatively low radiated power available from Magellan (Table 1), we restricted the observations to a geometry in which the incident and emerging ray directions lay in the same vertical plane (the scattering plane) and made equal angles to the surface, taking advantage of the scattering enhancement associated with specular reflection. Equally important was the applicability of the

Table 1. Magellan bistatic radar characteristics.

Parameter	Value
Magellan spacecraft transmitter	
Frequency	2.298 GHz
Wavelength	13.05 cm
Polarization	Linear
CW power	5 W
Antenna gain (3.7-m diameter)	35.9 dB
Antenna beamwidth	2.1° by 2.5°
Earth receiver (DSN DSS63)	
Antenna gain (70-m diameter)	63.3 dB
System temperature (viewing Venus)	20 K
Polarization	Left-right circular

G. H. Pettengill and P. G. Ford, Center for Space Research, Massachusetts Institute of Technology, Cambridge, MA 02139, USA.
R. A. Simpson, Center for Radar Astronomy, Stanford University, Stanford, CA 94305, USA.

*To whom correspondence should be addressed.

Fresnel scattering equations (6) to this geometry, which permitted unambiguous theoretical modeling of the results. The surface regions accessible to study were determined by the spacecraft's orbit, the relative positions of Venus and Earth, and the rotational phase of Venus. Only in early June 1994 were these geometric constraints fulfilled for Maxwell Montes, an extensive region known for anomalously low values of thermal emission.

We carried out bistatic radar observations on 5 June 1994, using the 70-m-diameter antenna of the NASA Deep Space Network (DSN) near Madrid, Spain, as the receiving system (Table 1). The linearly polarized S band high-gain transmitting antenna on the spacecraft was continuously directed at the region on the Venus surface that satisfied the conditions for specular reflection as seen from Earth. The direction of incident polarization was maintained at 45° to the scattering plane, thus ensuring equal in-phase excitation of the parallel (in-plane) and perpendicular (normal-to-plane) Fresnel reflection components. Three orbital passes, separated by twice the orbital period of the spacecraft (about 2 × 93 min), used the S band system to view a surface strip extending northward from near the Venus equator and passing over Maxwell Montes (Fig. 1). The interleaved passes used Magellan's shorter wavelength X band telemetry carrier, but these passes did not yield detectable echoes, probably because of the large atmospheric absorption at the shorter wavelength. The received data were recorded and processed digitally (7) to obtain a Stokes vector description (8) of the intensity and polarization of the echoes.

The results for most surface regions below an altitude of 6054 km (except near 65.5°N) (Table 2) imply a surface having a real dielectric permittivity of 4.0 ± 0.5 (Fig. 2), consistent with earlier results deduced from emissivity data (1, 2). The behavior of the echo from Maxwell Montes, however, is different (Fig. 3). The polarization angle (7) decreased as the specular reflection point entered the low-emissivity Maxwell highlands at about 61°N. Initially the echo was weak, incurring large measurement errors in the polarization angle, but as the track passed by the prominent crater Cleopatra near 65.5°N (Fig. 1), the signal intensity increased, presumably a result of a smoother surface. In this area, the polarization angle averaged −36.9° ± 2° at an incidence angle of 67.0° (68.5° before correcting for refraction) (Tables 2 and 3). This angle is in contrast with a polarization angle of +5.7°, that would be expected for a dielectric permittivity of 4.0 at a similar incidence angle. Furthermore, 10% of the echo power from this region is right circularly polarized. Combining these observed parameters with the value of emissivity, 0.33, measured earlier for Maxwell Montes by the Magellan radiometer at an emergence angle of 45° (1), permits an estimate of dielectric permittivity.

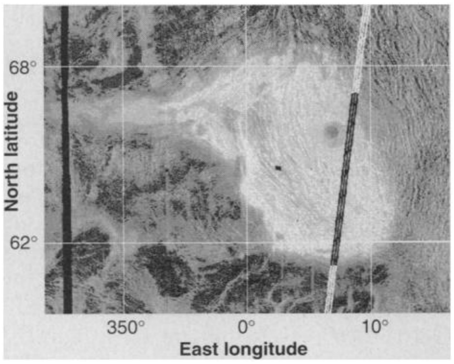

Fig. 1. Track of the specularly reflecting region over the Venus surface observed during the three S band bistatic radar passes of 5 June 1994. The extended bright feature represents the elevated Maxwell Montes, with the impact crater Cleopatra to the upper right.

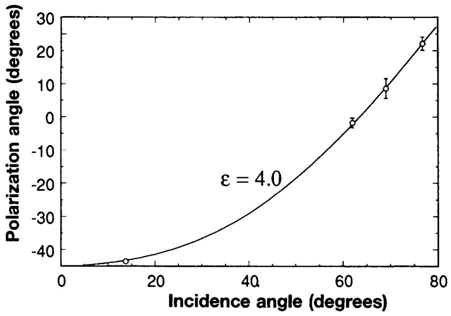

Fig. 2. Plot of polarization angle versus angle of incidence, for a dielectric permittivity ε of 4.0. Circles indicate observed data (with errors) from those locations in Table 2 not located in Maxwell Montes.

It is clear from the large negative polarization angle that the specularly reflecting surface must have a high relative dielectric permittivity. The generation of circular polarization requires a complex permittivity, implying a finite phase shift (other than 0° or 180°) between the reflected components parallel and perpendicular to the scattering plane. Such a shift can arise only if there is loss in the reflection process.

The Fresnel (amplitude) reflection coefficients are complex numbers given by (6)

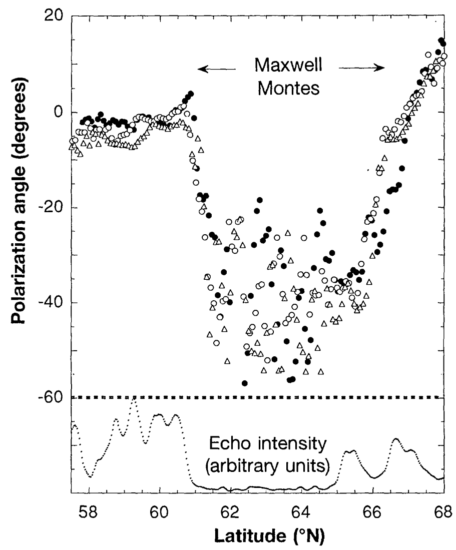

Fig. 3. Plot of the average received echo power (arbitrary linear units) and polarization angle in the Maxwell Montes region for the three S band orbital passes of 5 June 1994. Filled circles represent data from the first orbital pass, open circles the second, and triangles the third.

Table 2. Observed parameters for selected reflecting locations on Venus. The three entries in each subgroup correspond to S band passes 1, 2, and 3, respectively.

Surface		Incidence angle* (degrees)	Polarization angle (degrees)	Circular polarization† (%)
Latitude (°N)	Longitude (°E)			
5.7	0.06	12.7	−42.8 ± 4	−1 ± 2
7.4	0.4	13.9	−43.4 ± 3	0 ± 2
7.7	0.6	14.0	−44.3 ± 4	0 ± 2
59.7	6.4	61.9	−0.2 ± 2	1 ± 2
59.7	6.6	61.9	−1.2 ± 2	−1 ± 2
59.7	6.8	61.8	−3.9 ± 2	0 ± 2
65.3	8.0	66.8	−34.5 ± 2	−10 ± 2
65.4	8.2	67.0	−37.7 ± 3	−9 ± 3
65.6	8.5	67.2	−38.6 ± 3	−11 ± 3
67.7	8.8	69.0	+10.1 ± 4	0 ± 2
67.7	9.0	69.0	+9.9 ± 3	−1 ± 2
67.7	9.2	68.9	+5.8 ± 3	0 ± 2
75.9	12.9	76.8	+21.9 ± 2	0 ± 2
75.9	13.2	76.8	+23.3 ± 3	0 ± 2
75.9	13.4	76.8	+15.4 ± 10‡	1 ± 2

*Corrected for refraction. †Negative sign indicates right-hand circular sense. ‡Strong adjacent frequency interference noted in this observation.

$$\rho_{\parallel} = \frac{\varepsilon\cos\theta - \sqrt{\varepsilon - \sin^2\theta}}{\varepsilon\cos\theta + \sqrt{\varepsilon - \sin^2\theta}} \quad (1)$$

$$\rho_{\perp} = \frac{\cos\theta - \sqrt{\varepsilon - \sin^2\theta}}{\cos\theta + \sqrt{\varepsilon - \sin^2\theta}}$$

where $\parallel$ refers to the parallel and $\perp$ to the perpendicular reflected components, ε is the complex relative dielectric permittivity, and θ is the angle of incidence (and reflection). The associated emissivities correspond to 1 minus the squared magnitude of $\rho_{\parallel}$ and $\rho_{\perp}$. We assumed that the emissivity observed over Maxwell Montes is the average value of the two polarization components, because the surface in this region is known to be highly depolarizing.

The circularly polarized fractional power, C, is related to the differential phase shift between the two coefficients, δ (in the sense: $\parallel$ minus $\perp$), by (8)

$$C = (\sin 2\gamma \sin\delta)^2 \quad (2)$$

where $\gamma = \tan^{-1}|\rho_{\parallel}/\rho_{\perp}|$. The polarization angle, A, of the linearly polarized component is given by

$$A = \frac{1}{2}\tan^{-1}(\tan 2\gamma \cos\delta) \quad (3)$$

The Stokes vector convention assigns a negative sign to C when the right circular sense predominates, as it does in our observations.

We have explored the complex reflection amplitudes associated with various real and imaginary components of the dielectric permittivity of a surface material and find the best agreement with our data for $\varepsilon = -i100$, with an error in $|\varepsilon|$ of less than 50 (Table 3). For the illumination geometry used here, with the incident linear polarization plane maintained to the upper left at 45° to the scattering plane as viewed from the spacecraft, the inferred value of $\delta = 162.1°$ at a refraction-corrected incidence angle of 67.0° (as compared to $\delta = 180°$ for a lossless dielectric viewed below its Brewster angle) yields a right circularly polarized sense, as observed. The discrepancy in emissivity may arise in part from the effects of a rough surface, which raise the emission efficiency as compared with the emissivity calculated for a smooth specular surface (9).

Table 3. Comparison between the average values of three observed parameters for the surface of a region in Maxwell Montes and the corresponding calculated values for a complex dielectric permittivity $\varepsilon = -i100$. The emissivity is polarization-averaged and calculated for an emission angle of 45°, whereas the polarization angle *A* and the percentage of circular power *C* correspond to an incidence angle of 67.0°.

Case	Emissivity (45°)	*A* (degrees)	*C* (%)
As observed	≈0.33	−36.9 ± 2	−10 ± 2
$\varepsilon = -i100$	0.26	−36.1	−8.7

The most likely explanation of the large imaginary component is a semiconducting surface material, where the relation between ε and conductivity, σ, is given by (6)

$$\varepsilon \cong -i\left(\frac{\sigma}{\omega\varepsilon_0}\right) = -i7.83\sigma \quad (4)$$

where σ is in mhos per meter, $\omega = 2\pi f$ is the angular frequency of the transmitted carrier, and ε_o is the permittivity of free space. For $\varepsilon = -i100$, $\sigma = 13$ mho/m, which is about 10^{-6} of the electrical conductivity of most metals and conducting minerals, and at least 10^{10} times the σ for insulators (10). Among the elements, only Ge, with $\sigma_{ge} \approx 20$ mho/m (10), and Te, with $\sigma_{te} \approx 2000$ mho/m, for low radio frequencies at temperature $T = 700$ K (11), have conductivities within a few orders of magnitude of our observations. Of the two elements, the more interesting is Te, with a melting-point temperature of 723 K (12) [Te is a liquid in the Venus lowlands (T = 730 to 750 K) (13) but a solid at Venus altitudes above about 6054 km]. In the lowlands, Te has a saturated vapor pressure of about 7×10^{-4} bar (11), which drops to below 10^{-5} bar in the Maxwell Montes highlands, where temperatures fall as low as 650 K. Thus, there could be a continuously recycling cold-trap deposition of Te from the vapor phase (14), if enough of it is available above an altitude of about 6054 km, the lowest altitude at which the anomalous electrical properties are observed. Compounds containing Te are found in volcanic effusions on Earth (14) and are probably brought to the surface on Venus by such processes, although the presence of elemental Te in these emissions has not been established.

How might we explain the 200-fold discrepancy between the inferred electrical conductivity of 13 mho/m and the estimated value of 2000 mho/m for Te at a temperature of 700 K? The values at high radio frequency might be less than at low frequencies as a result of the finite number of charge carriers in a semiconductor such as Te. Note also that we have deduced the value of conductivity from the observed dielectric permittivity, assuming a surface layer thickness greater than the electrical skin depth (15) of 3.0 mm for the S band wavelength used here. A thinner surface deposition would yield a lower effective conductivity. If the conductivity for a thick layer of Te is actually 2000 mho/m, then the corresponding skin depth is 0.3 mm, and a layer about 5 μm thick would have a conductivity of 13 mho/m. If we assume the terrestrial abundance of about 16×10^{-9} for Te (16) throughout the mantle and crust of Venus, it would require outgassing of less than 1 part in 10^{-4} to saturate the atmosphere over the highlands.

The high dielectric permittivity found on Maxwell Montes rules out volume scattering (3) as the controlling factor in producing low emissivity in the highlands, although the large depolarizations seen in radar echoes there may arise from dual scattering from highly reflective, wavelength-scale deep structure on the surface (17). Wood (18) has proposed a plating of pyrites or magnetite as a source of conducting material, and Shepard *et al.* (19) have shown that ferroelectrics may also have the electrical properties needed to account for the radar observations. Both of these types of material require substantial loss mechanisms if they are responsible for the bistatic observations. Until spacecraft probes have sampled the surface in the highlands, the composition of this region will probably remain uncertain.

REFERENCES AND NOTES

1. G. H. Pettengill, P. G. Ford, S. Nozette, *Science* **217**, 640 (1982); P. G. Ford and G. H. Pettengill, *ibid.* **220**, 1379 (1983); G. H. Pettengill, P. G. Ford, R. J. Wilt, *J. Geophys. Res.* **97**, 13091 (1992).
2. G. H. Pettengill, P. G. Ford, B. D. Chapman, *J. Geophys. Res.* **93**, 14881 (1988); G. L. Tyler *et al.*, *Science* **252**, 265 (1991); G. L. Tyler, R. A. Simpson, M. J. Maurer, E. Holmann, *J. Geophys. Res.* **97**, 13115 (1992).
3. K. A. Tryka and D. O. Muhleman, *J. Geophys. Res.* **97**, 13379 (1992); R. J. Wilt, thesis, Massachusetts Institute of Technology (1992).
4. R. A. Simpson, *IEEE Trans. Geosci. Remote Sensing* **31**, 465 (1993).
5. R. S. Saunders *et al.*, *J. Geophys. Res.* **97**, 13067 (1992).
6. J. A. Stratton, *Electromagnetic Theory* (McGraw-Hill, New York, 1941).
7. The transmitting waveform at both S and X band wavelengths was continuous (CW), with the echoes recorded simultaneously in a pair of orthogonal, circularly polarized coherent receivers at a digital sampling rate of 50,000 8-bit words/s, a rate that satisfied the Nyquist condition for the 25-kHz filtered bandwidth. The local oscillator of the receiver was adjusted to maintain the approximately 2-kHz-wide echo within the receiving bandwidth at all times. We analyzed the recorded data using a complex fast-Fourier transform and temporal averaging to recover the Stokes parameters (8) for each of 128 195.3-Hz-wide spectral components spanning the 25-kHz receiver bandwidth. Further convolution of these data incoherently in time and frequency improved the signal-to-noise ratio and allowed estimates of the position angle of the received plane of polarization (the polarization angle), as well as of the intensities of the linear and circularly polarized components of echo power, at 1-s intervals over the approximately 24-min duration of each pass. Data were also taken at times when the spacecraft antenna was directed toward Earth in a known orientation, to provide an attitude and intensity reference for receiver phase and amplitude calibration. The primary reference for recovering the absolute polarization angle was based on observations of the spacecraft's signal while its antenna pointed directly at Earth. Faraday rotation during these observations varied from about 3° to 1° (A. Coster, personal communication). Its variation over the observing interval (observed to be less than ±2° from the average over the

6-hour observing interval) has been neglected, except as a contribution to the measurement error; in any event, the variation could not be distinguished from possible drifts in the relative phases of the two DSN receivers. The circularly polarized receiver levels were set to yield equal values for the linearly polarized received signal during periods of direct pointing toward Earth; the absence of significant circular polarization in the echo (except over Maxwell Montes) is taken as evidence that this procedure was valid. We believe that small delay differences in the 15-dB receiver attenuators, present during direct downlink but removed during reception of the echo, may be responsible for a bias of a few degrees of electrical phase deduced from the polarization rotation observed at small angles of incidence. In any event, we have increased all of the "raw" values of polarization angle, as obtained from the primary reference, by an estimated 2.7° of bias, in order to bring the average value of the observed polarization angles for reflection from the "normal" surface at 13.7° incidence to its anticipated theoretical value of −43.5° (this value is quite insensitive to the precise value of the dielectric constant at this low incidence, and these data provide our secondary reference).

8. J. D. Kraus, *Radio Astronomy* (Cygnus-Quasar, Powell, OH, 1986), pp. 4–14.
9. F. T. Ulaby, R. K. Moore, A. K. Fung, *Microwave Remote Sensing* (Artech House, Norwood, MA, 1982), vol. 2.
10. *Handbook of Chemistry and Physics* (Chemical Rubber Publishing, Cleveland, 1973), p. F-145; G. R. Olhoeft, in *Physical Properties of Rocks*, Y. S. Touloukian, W. R. Judd, R. F. Roy, Eds. (Hemisphere Publishing, New York, 1989), p. 257.
11. W. M. Becker and V. A. Johnson, in *Chemistry of Selenium, Tellurium, and Polonium*, K. W. Bagnall, Ed. (Elsevier, Amsterdam, 1966), chap. 3.
12. *Handbook of Chemistry and Physics* (Chemical Rubber Publishing, Cleveland, 1973), p. D-142.
13. A. Seiff *et al.*, *J. Geophys. Res.* **85**, 7903 (1980).
14. R. A. Brackett, B. A. Fegley Jr., R. E. Arvidson, *ibid.* **100**, 1553 (1995).
15. The "skin depth" represents the distance, *d*, into the conducting surface at which the penetrating electromagnetic wave is reduced to 1/*e* of its external value; it is given by (*6*)

$$d = \sqrt{\frac{2}{\omega\sigma}}$$

16. J. S. Kargel and J. S. Lewis, *Icarus* **105**, 6 (1993).
17. B. Hapke, *ibid.* **88**, 407 (1990).
18. J. A. Wood, in *Venus II*, S. Bougher, D. Hunten, R. Phillips, Eds. (Univ. of Arizona Press, Tucson, in press).
19. M. K. Shepard, R. E. Arvidson, R. A. Brackett, B. A. Fegley Jr., *Geophys. Res. Lett.* **21**, 469 (1994).
20. We thank the staff of the NASA DSN, as well as the dedicated engineers of the Jet Propulsion Laboratory (JPL) and Lockheed-Martin Aerospace, for their painstaking support in implementing this complex experiment. This work was supported under NASA grants NAGW-3787, NAGW-4351, and NAGW-3702 and JPL contracts 959490 and 957089.

11 December 1995; accepted 23 April 1996

High-Resolution Molecular Spectroscopy of van der Waals Clusters in Liquid Helium Droplets

Matthias Hartmann, Roger E. Miller,* J. Peter Toennies,†
Andrej F. Vilesov

Small van der Waals clusters of sulfur hexafluoride (SF_6) and mixed SF_6–rare gas clusters were prepared inside large droplets of helium-4, with each droplet consisting of about 4000 helium atoms. A diode laser was used to measure the high-resolution infrared spectra of these clusters in the vicinity of the ν_3 vibrational mode. In all cases rotational structure was observed, indicating that the embedded species rotate nearly freely, although they had been cooled to a temperature of 0.37 kelvin. The results indicate that helium droplets are probably superfluid and thereby provide a uniquely cold yet gentle matrix for high-resolution spectroscopy.

Spectroscopy has contributed greatly to our understanding of molecular behavior, but unfortunately many of the methods are ineffective when applied to complex molecules because of spectral congestion (vibrational and rotational) that blurs the details. For this reason, free jet expansions are widely used to simplify spectra by cooling molecules (*1*). Nevertheless, for large molecules the heat capacity may be so large that the cooling is incomplete. Although ultracold solid matrices (*2*) overcome this limitation, the matrix interactions can significantly perturb the spectrum (*2, 3*). From this point of view, liquid He would be the ideal matrix, except for the fact that the solvated molecules are quickly lost to the container walls (*4–6*). This problem can be overcome if the molecules are captured inside small droplets of liquid He, thus providing the needed isolation (*7–9*). Reported here are high-resolution spectra (0.01 cm^{-1}) of a number of He-solvated molecules, clusters, and van der Waals complexes that demonstrate that this is a viable approach for carrying out ultracold spectroscopy of large molecules. The results show that the solvent effects are weak yet interesting in their own right and that the solvated species are cooled to the temperature of the liquid droplets (0.37 K).

We have previously studied the case of a single SF_6 molecule in a He droplet (*9, 10*). We concluded that the molecule was solvated inside the droplet in a homogeneous environment, as deduced from mass spectrometer experiments (*11*) and predicted by theory (*12–14*). This is in contrast with the idea that the SF_6 molecule is positioned at an asymmetric surface site [this hypothesis was proposed earlier on the basis of low-resolution infrared studies (*8*)]. The vibrational hot bands of SF_6, which are observed even in the free jet expansion spectra (*15*), were completely absent in our spectrum, indicating that the cooling was complete. These results suggested that liquid He droplets may provide an ultracold, gentle matrix in which molecules are free to rotate and that the detailed rotational structure may provide insights into the interactions between the liquid He and the trapped molecule. We found from the rotational structure of the SF_6 spectrum that the temperature of the ^4He droplet was $T = 0.37$ K. Nevertheless, in considering the generality of the method, one might argue that the spherical symmetry of the SF_6 molecule is ideally suited to minimizing the interaction with the He and that this example may not be representative of the general case. Rather than switching to a different molecule to address this issue, we chose to study van der Waals complexes of SF_6, for example, the dimer of SF_6 which has been studied extensively in free jet expansions (*16, 17*) and at low resolution in liquid He (*8*).

The experimental apparatus used in the present study has been described previously (*9, 10*) (Fig. 1). We introduced SF_6 molecules into the He droplets using a "pick-up" method (*18*). Once formed, the droplets passed through a scattering chamber where the gas of interest, SF_6, was added at a known pressure, typically 10^{-5} mbar. The average number of molecules captured by the He droplet depends directly on this pressure (*19*). Upon capturing a hot SF_6 molecule, the droplet rapidly evaporates He atoms from its surface, and after approximately 10^{-6} s, the temperature returns to the initial droplet temperature, cooling the captured molecule. Of the ~4000 He atoms that make up the droplet (*20*), about 600 evaporate during the capture process (*19*).

The SF_6-containing He droplets were detected by electron impact ionization in a quadrupole mass spectrometer. By far the most probable event is ionization of a He atom in the droplet, followed by resonant charge transfer with neighboring atoms until the charge localizes on the SF_6 molecule (*11*). This charge localization usually results in the complete evaporation of the remaining He droplet, owing to the release of the large difference in the ionization energies of He and SF_6 to the cluster. The largest ion signals were observed at the mass of the major SF_6 ion fragment, namely, SF_5^+. A semiconductor diode laser was used to ex-

Max-Planck-Institut für Strömungsforschung, Bunsenstraße 10, D-37073 Göttingen, Germany.

*Permanent address: Department of Chemistry, University of North Carolina, Chapel Hill, NC 27599, USA.
†To whom correspondence should be addressed.